Soliton and rogue wave statistics in supercontinuum generation in photonic crystal fibre with two zero dispersion wavelengths

Bertrand Kibler, Christophe Finot, John M. Dudley

EPJ manuscript No.
(will be inserted by the editor)

Soliton and rogue wave statistics in supercontinuum generation in photonic crystal fibre with two zero dispersion wavelengths

Bertrand Kibler,[1] Christophe Finot[1] and John M. Dudley[2]

[1] Institut Carnot de Bourgogne, UMR 5029 CNRS-Université de Bourgogne, 9 Av. A. Savary, Dijon, France
[2] Institut FEMTO-ST, UMR 6174 CNRS-Université de Franche-Comté, Route de Gray, Besançon, France.

Abstract. Stochastic numerical simulations are used to study the statistical properties of supercontinuum spectra generated in photonic crystal fibre with two zero dispersion wavelengths. For picosecond pulse excitation, we examine how the statistical properties of solitons generated on the long wavelength edge of the supercontinuum ("optical rogue waves") are modified by energy transfer to dispersive waves across the second zero dispersion wavelength. The soliton statistics (characterized in terms of peak power, wavelength and pulse duration) are shown to be strongly modified by the mechanism of dispersive wave generation, with the detailed form of the probability distribution depending strongly on input pulse energy.

1 Introduction

Supercontinuum (SC) generation in photonic crystal fibres (PCF) has been extensively studied in recent years [1]. For SC generation seeded by femtosecond pulses, the underlying spectral broadening mechanisms and noise properties are generally well understood, and research is now shifting towards studies in the so-called "long pulse" regime, using picosecond to nanosecond pump pulses, or quasi-continuous wave sources [2,3]. SC generation with long pulses has been shown to be associated with a rich variety of effects, including spontaneous pulse break up due to modulation instability (MI), collective soliton dynamics and collisions, and even incoherent turbulent dynamics that yields an effective field thermalisation [4,5]. Additional results that have received widespread attention concern experimental and numerical studies of "optical rogue waves," statistically rare extreme red-shifted Raman solitons which emerge from the long wavelength edge of the SC spectrum and which exhibit extreme value non-Gaussian statistics [6]. Subsequent studies have shown that control of the rogue wave fluctuations can be attained through the use of a weak seed stimulus to induce the initial phase of SC generation [7–10], whilst further work is extending the study of extreme value fluctuations to other systems such as silicon photonic devices and Raman amplifiers [11,12].

In the context of fiber SC generation, these extreme value statistics have been observed by studying the intensity characteristics of Raman solitons on the long wavelength edge of the SC generated in fibres with only one zero dispersion wavelength (ZDW) [6,7]. It is well known, however, that the use of PCF with two ZDWs significantly modifies the SC generation process, with the Raman self-frequency shift experienced by long wavelength solitons being arrested by the transfer of energy across the ZDW to a dispersive wave in the normal dispersion regime [13–15]. It would be expected that these modified dynamics would impact on the corresponding

soliton statistical properties, and our objective here is to examine this question in detail. Our main result is that the long wavelength soliton statistics are indeed significantly modified in a fibre with two ZDWs, and the probability distribution of soliton intensity can exhibit Gaussian, uniform, or extreme value characteristics depending on the pump energy regime considered. These results are significant both for an improved understanding of the nonlinear dynamics of supercontinuum spectral broadening, as well as being of potential importance for the selection of stabilised supercontinuum sources for particular applications [16].

2 Numerical simulations and illustrative results

Our analysis is based on the numerical simulation of the generalised non-linear Schrödinger equation [1] :

$$\frac{\partial A}{\partial z} + \frac{\alpha}{2}A - \sum_{k\geq 2} \frac{i^{k+1}}{k!}\beta_k \frac{\partial^k A}{\partial T^k} =$$

$$i\gamma\left(1 + i\tau_{shock}\frac{\partial}{\partial T}\right) \times \left[A(z,T)\int_{-\infty}^{+\infty} R(T')|A(z,T-T')|^2 dT'\right] \quad (1)$$

Here, A(z,T) is the field envelope and the left-hand side of this equation models linear propagation effects, with α the linear loss and the β_k's the usual dispersion coefficients. The right-hand side models nonlinear effect with γ the usual nonlinear coefficient. The response function $R(t) = (1 - f_R)\delta(t) + f_R h_R(t)$ includes both instantaneous electronic and delayed Raman contributions, with $f_R = 0.18$ representing the Raman contribution to the nonlinear response. The time derivative term on the right-hand side models the dispersion of the nonlinearity. This is characterized by a typical timescale of shock which includes the additional dispersion in the nonlinear response due to the frequency-dependence of the fibre mode area. This is particularly important in quantitatively modelling the self-frequency shift to the infrared experienced by the rogue solitons [17]. Noise is included in the frequency domain through a one photon per mode background. Further details of the numerical model can be found in [1].

We first compare the general statistical features of SC generation in a two-ZDW fiber with the more well-established case of SC in a single-ZDW fiber. We consider in particular the effect of input pulse noise on both the spectral and temporal properties of the output SC. Figure 1(ab1) shows the dispersion curves of the two fibres considered. PCF A (black line) is similar to the commercially-available fibre Crystal Fiber NL-PM-750, with two ZDWs at 750 nm and 1230 nm [15]. The nonlinear coefficient at the 890 nm pump wavelength considered here is $\gamma = 0.09\ W^{-1}m^{-1}$. PCF B (gray dashed line) is a typical PCF adapted for SC generation with a single ZDW at 750 nm and no second ZDW in the wavelength range studied [1]. Its nonlinear coefficient is taken identical to that of PCF A. We consider Gaussian input pulses of 1 ps duration (FWHM) propagating over a distance of 2 m in both cases. To examine the sensitivity of the SC dynamics to input pulse noise, we generate an ensemble of 1000 simulations in the presence of different random noise at a level corresponding to 1% shot-to-shot fluctuations in initial peak power.

For an input energy of 200 pJ, the remaining subfigures of Fig. 1 show the results obtained from our simulations. For PCF A (two ZDWs) the spectral and temporal characteristics are shown in Figs 1(a2) and (a3) respectively. For PCF B (single ZDW) the corresponding results are shown in Figs 1(b2) and (b3) respectively. In both cases we superpose results from the individual realisations in the ensemble (gray curves) together with the calculated mean (black). For clarity we show only 200 results from the ensemble in the figure.

For both PCF A and PCF B, with picosecond pump pulses in the anomalous dispersion regime, SC generation develops from an initial phase of unpredictable pulse break up due to MI, followed by the generation of a series of distinct soliton pulses that subsequently move to longer wavelengths through the Raman soliton self-frequency shift effect. The spectral and temporal characteristics of these generated solitons are apparent from the results shown in Figure 1. Several features of these curves are significant. The solitons are generated sequentially from

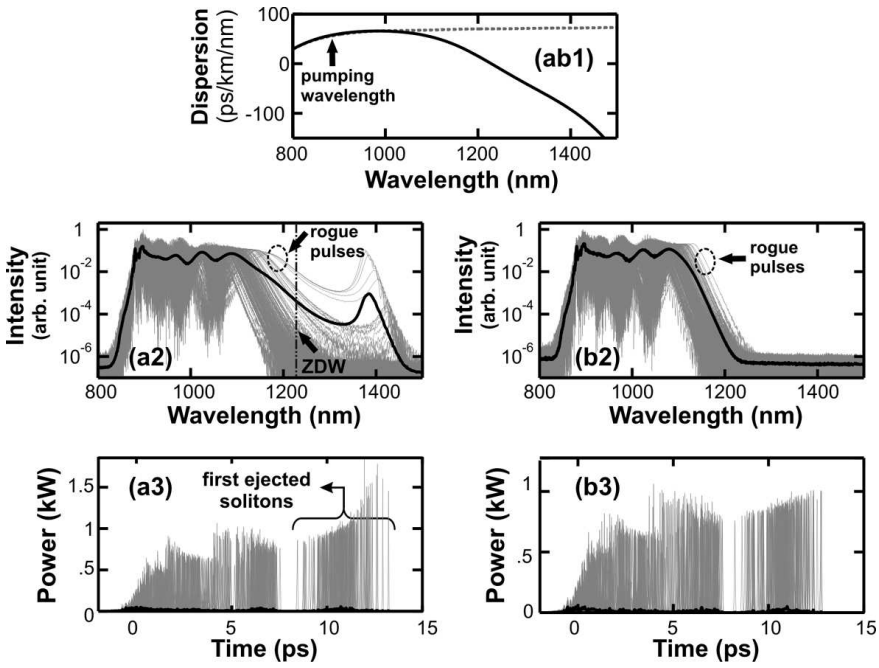

Fig. 1. (ab1) Dispersion profile of the fibers under study: PCF A (solid black line) and PCF B (dashed gray line). The remaining subfigures show simulation results for SC obtained for input pulse energy of 200 pJ. Spectral (a2,b2) and temporal (a3,b3) average intensity profiles (black lines) are compared with the superposition of 200 individual simulation results (gray traces). Left column (a2,a3) corresponds to results for PCF A, right column (b2,b3) corresponds to results for PCF B.

the breakup of the initial pulse, but the effect of noise on this process results in significant jitter in the position of the first ejected soliton. Nonetheless, as shown in Fig. 1(a2), we can readily distinguish distinct sets of ejected solitons, and this allows us to use a numerical temporal gating procedure to isolate these solitons and examine their statistical properties in more detail. Secondly, as is clear from inspection of Fig. 1, the presence of the second-ZDW in PCF A results in significant energy transfer to longer wavelengths, as a portion of the soliton energy is transferred to a dispersive wave as it shifts to the vicinity of the second ZDW [18,19]. We also note that the fluctuations in the ejected soliton characteristics feed into the amplitude of the generated dispersive wave.

As discussed above, a convenient and straightforward way to quantify the statistical behaviour of the SC fluctuations is in terms of the characteristics of the first ejected solitons. We now present some illustrative results to show how this technique can be used to examine the SC fluctuations in more detail. These results are shown in Figure 2. Here we compare the statistical properties of the peak powers of the first ejected solitons for SC generated in PCF A (two ZDWs) and PCF B (single ZDW) for four initial pulse energies (150, 200, 275, 330 pJ). In particular, for each realisation in the ensemble, we identify the first ejected soliton through numerical temporal gating, which allows us to determine its peak power. Analysis over the ensemble allows us to build up the corresponding probability histograms, and these results are shown in the subplots (a1-a4) for PCF A and subplots (b1-b4) for PCF B.

For both fibres, the form of the histograms exhibits clear dependence on pulse energy. At low energies [Fig. 2(a1) and (b1)] the distributions are near-Gaussian in both cases, with no significant tail. As the initial energy increases, however, the qualitative nature of the distribution changes. In the case of the single-ZDW fibre (PCF B), increased pulse energy leads to increasing asymmetry in the histogram and evolution towards the "L-shaped" optical rogue wave characteristic [6]. On the other hand, the results for the two-ZDW fibre (PCF A) are significantly different. Specifically, although L-shaped asymmetric spectra are seen in Figs 2(a2) and (a4),

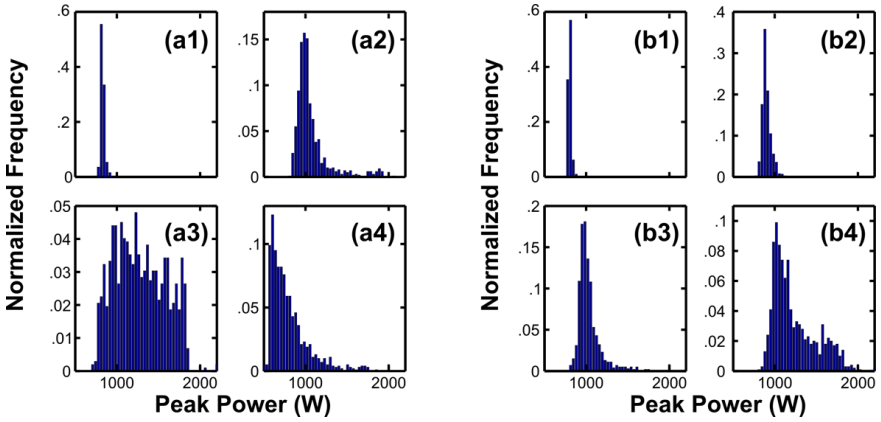

Fig. 2. Statistical distributions of the peak-power of the first red-shifted soliton are plotted on subplots (1-4) for initial pulse energy of 150, 200, 275, 330 pJ respectively. Results for PCF A and B are plotted on subplots (a) and (b) respectively. Note the extreme dependence of the histograms on pulse energy in both cases.

the intermediate energy case shown in Fig. 2(a3) exhibits a near uniform distribution, implying a similar probability of observing solitons with peak power varying over the range 600-1800 W. Additional simulations over a wider parameter range have confirmed that this behaviour is a specific and unique feature of SC generation and soliton ejection in fibres with two ZDWs, and we therefore consider this in more detail in the following section.

3 Soliton statistical properties and dependence on initial energy

To examine the statistical properties of SC generation in PCF A in more detail, we consider similar results to those shown in Fig. 2, but over a continuous range of pump energies from 130 to 380 pJ. This corresponds to an input soliton order varying over the range 13-23. These results are shown in Figure 3, where we plot the histograms using a grayscale representation as explained in the caption. The figure shows histograms of (a) soliton intensity and (b) soliton wavelength for a continuous range of pump energies, and the advantage of this representation is that it allows us to readily identify three broad regimes.

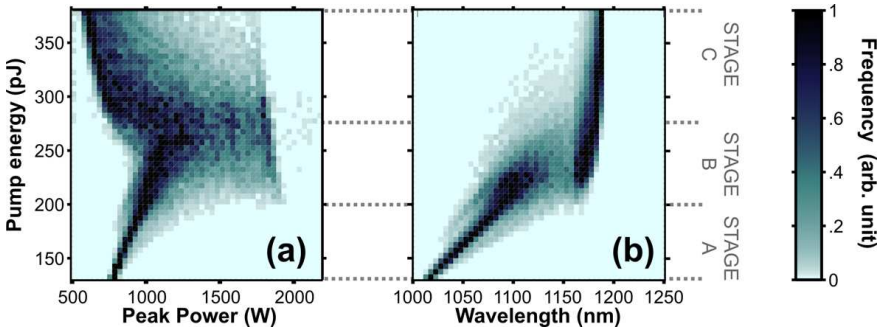

Fig. 3. Evolution with pump energy of the statistical distributions of the peak-power (a) and the central wavelength (b). Grayscales are normalized to 1 for the highest probability. The distribution for a given energy is obtained from a set of 1000 simulations for PCF A. Note that three regimes of pump energies can be clearly identified, showing different statistical properties of the first ejected solitons.

Firstly, Stage A corresponds to "orthodox" SC generation where there is long wavelength Raman soliton generation, but the interaction with the second ZDW does not significantly impact on the dynamics. This stage is qualitatively similar to the dynamics which could be observed in a single-ZDW fibre. As a result we see evolution from initially Gaussian-distributed pulse peak power to the long-tailed rogue wave distribution described in [6–8]. Secondly, Stage B occurs at the point where the solitons approach the second ZDW and their frequency begins to stabilize. Because the energy transfer mechanism itself depends on soliton proximity to the ZDW [13], this flattens the probability distribution of soliton amplitudes as it is the more intense solitons that are closer to the ZDW and thus it is these that preferentially transfer energy to the dispersive waves. Finally, Stage C occurs when the bulk of the solitons have transferred their energy across the ZDW and the distribution tail therefore corresponds to those that have not yet reached the vicinity of the ZDW.

In order to gain further insight into the red-shifting soliton dynamics, Fig. 4(a) plots similar results to those shown above, but this time showing a histogram of the temporal width (FWHM) of the ejected solitons. We note the same three stages as in Fig. 3. In Stage A, the peak of the histogram shifts to shorter temporal widths. This arises because as the pulses shift to longer wavelengths, the (absolute value) of the local dispersion value progressively decreases, leading to pulse compression in order to maintain a constant soliton number [20]. A direct consequence of this temporal compression is a peak power increase - in fact this can be seen earlier in Fig. 1(a3) where the most red-shifted solitons (which are also the most delayed pulses) exhibit a noticeably higher intensity. In stage B at higher input pulse energies, the distribution of temporal widths becomes bimodal: for this case the region 25-30 fs corresponds to pulses which have already been stabilized by the dispersive wave, whereas the region 40-50 fs contains pulses which have not reached the vicinity of the ZDW yet. Finally, in Stage C at the largest pulse energies, we see that this latter zone effectively disappears as all the solitons reach close enough to the ZDW to experience dynamical stabilisation due to dispersive wave energy transfer. We can also note that the distribution in the region 25-30 fs is continuously shifting to larger pulse values at the end of stage C due to the continuous energy transfer from solitons to DW.

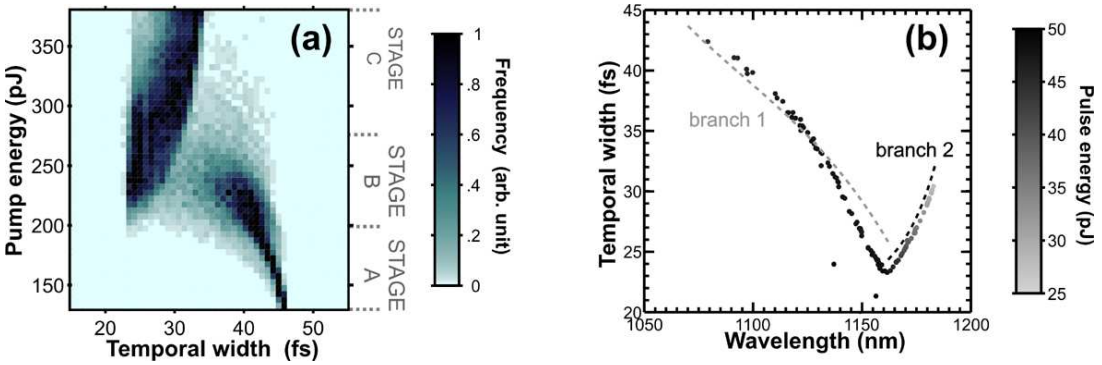

Fig. 4. (a) Evolution with pump energy of the statistical distributions of the temporal width of the first red-shifted soliton. The grayscale is normalized to 1 for the highest probability. Distribution for a given energy is the result obtained from a set of 1000 simulations for PCF A. (b) Evolution of the FWHM temporal width of the red-shifted solitons as a function of wavelength for an initial pulse energy of 275 pJ. The results are compared with predictions based on Eq. 2 taking N = 1.15 and N = 1.11 for branch 1 and 2 respectively (gray dashed lines and black dashed lines respectively), in particular the superposition of 100 representative individual shots for the sake of clarity. Note that the grayscale axis on the figure illustrates the energy variation of solitons due to their energy transfer to dispersive waves.

Figure 4(b) confirms this analysis by considering a particular input pulse energy of 275 pJ, and examining the ensemble results on a shot-by-shot basis. For each result in the ensemble,

we plot the temporal duration against central wavelength. Two distinct branches can clearly be observed and the behavior shown can be interpreted by the following relation derived from the usual soliton condition:

$$T_{FWHM} = 3.53N^2 \frac{|\beta_2(\lambda)|}{\gamma E} \tag{2}$$

Here E is the pulse energy and $\beta_2(\lambda)$ is the second order dispersion at the central wavelength λ of the red shifted pulse.

Along branch 1, although there is significant scatter in wavelength and pulse duration, the red-shifted soliton pulses are nonetheless found to possess near-identical energies. The calculated soliton-order for each pulse along this branch is close to the value of a fundamental soliton, and thus we interpret the points on this branch as corresponding to solitons that have emerged from the initial MI phase and shifted to longer wavelengths. The scatter arises from the stochastic nature of the initial MI, but for each soliton in the ensemble (i.e. each point along this branch), the temporal width is determined by the dispersion at the central wavelength of the pulse $\beta_2(\lambda)$. Specifically, because the highest power solitons reach longer central wavelengths with lower local dispersion value in PCF A, they evolve to a shorter temporal pulse duration in order to maintain a constant soliton number [20]. The dashed line in the figure shows the expected variation of temporal width with wavelength calculated from Eq. (2) using the dispersion characteristics of the fibre.

The behavior along the second branch of this curve is, on the other hand, very different. Here the extracted solitons at different wavelengths possess not only different pulse durations but also different energies. This is because solitons along this branch (which plots behavior at longer wavelengths) undergo energy loss to the dispersive wave generated in the normal dispersion regime at wavelengths longer than the second ZDW at 1230 nm. As the solitons lose energy, their temporal width increases to compensate and maintain a soliton number close to 1 (in fact N is estimated as 1.11 for branch 2). Because of the energy variation with wavelength due to dispersive wave generation, the different points along the branch are plotted in different shades of gray referenced to the energy grayscale shown. Note that this energy grayscale also applies to the points along branch 1, but no energy variation is apparent on this branch because the solitons have constant energy.

4 Conclusions

The dynamics of SC generation in optical fibre are complex. It is only recently that the implications of this complexity on the statistical properties of the SC spectra has been appreciated, but there is clearly much interest in developing a more complete understanding of the underlying physical mechanisms that induce SC instabilities, especially fluctuations in solitons ejected from an initial phase of modulation instability.

Our primary intention in this paper has been to study the statistical properties of the first red-shifted ejected solitons generated during picosecond continuum generation in a two zero-dispersion wavelength PCF. Depending on the initial pulse energy, various distributions including both L-shaped extreme-value and near-uniform histograms have been reported.

Extensive simulations have outlined the crucial role played by the stabilization of the frequency-shifted pulses near the second ZDW. The essential physical mechanism underlying the appearance of such a uniform distribution of soliton amplitudes is straightforward to understand: for a certain range of input powers, we are in a regime corresponding to the onset of dispersive wave transfer where the more intense solitons in the distribution Raman-shift to the zero dispersion wavelength first and thus preferentially lose energy to the dispersive wave.

This observation is clearly of interest in understanding the noise properties of SC generated in fibres with two ZDWs, and may also have important practical consequences. In particular, for applications such as certain classes of micromachining where ultrashort pulses are used for non-resonant excitation, the use of a two-ZDW PCF may prove useful in generating amplitude-stabilised femtosecond pulses from an initial picosecond source excitation.

5 Acknowledgments

This work was supported by the Agence Nationale de la Recherche (ANR MANUREVA, SOFICARS and PERSYST II projects: ANR-08-BLAN-0401-01, ANR-07-RIB-013-03 and ANR-07-TCOM-014), by the Conseil Rgional de Bourgogne, and was carried out within the framework of the Research Networks GDR Phonomi2, COST action 299 FIDES and PRES UFC-UB.

References

1. J. M. Dudley, G. Genty, and S. Coen, Rev. Mod. Phys. **78**, 1135-1184 (2006).
2. C. Xia, M. Kumar, M.-Y. Cheng, O. P. Kulkarni, M. N. Islam, A. Galvanauskas, F. L. Terry, M. J. Freeman, D. A. Nolan, and W. A. Wood, IEEE J. Sel. Top. Quantum Electron. **13**, 789-797 (2007).
3. B. A. Cumberland, J. C. Travers, S. V. Popov, and J. R. Taylor, Opt. Express **16**, 5954-5962 (2008).
4. B. Barviau, B. Kibler, S. Coen, and A. Picozzi, Opt. Lett. **33**, 2833-2835 (2008).
5. B. Barviau, B. Kibler, A. Kudlinski, A. Mussot, G. Millot, and A. Picozzi, Opt. Express (in press, 2009).
6. D. R. Solli, C. Ropers, P. Koonath, and B. Jalali, Nature **450**, 1054-1057 (2007).
7. J. M. Dudley, G. Genty, and B. J. Eggleton, Opt. Express **16**, 3644-3651 (2008).
8. G. Genty, J. M. Dudley, and B. J. Eggleton, Appl. Phys. B **94**, 187-194 (2009).
9. D. R. Solli, C. Ropers, and B. Jalali, Phys. Rev. Lett. **101**, 233902 (2008).
10. A. Efimov and A. J. Taylor, Opt. Express **16**, 5942-5953 (2008).
11. D. Borlaug and B. Jalali, 21st Annual Meeting of the IEEE Lasers and Electro-Optics Society, Newport Beach, USA, 9-13 Nov. 2008.
12. K. Hammani, C. Finot, J. M. Dudley, and G. Millot, Opt. Express **16**, 16467-16474 (2008).
13. D. V. Skryabin, F. Luan, J. C. Knight, and P. St. J. Russell, Science **301**, 1705-1708 (2003).
14. P. Falk, M. H. Frosz, O. Bang, L. Thrane, P. E. Andersen, A. O. Bjarklev, K. P. Hansen, and J. Broeng, Opt. Lett. **33**, 621-623 (2008).
15. B. Kibler, C. Finot, G. Gadret, G. Millot, J. Wojcik, M. Szpulak, and W. Urbanczyk, Electron. Lett. **44**, 1370-1371 (2008).
16. E. R. Andresen, V. Birkedal, J. Thogersen, and S. R. Keiding, Opt. Lett. **31**, 1328-1330 (2006).
17. B. Kibler, J. M. Dudley, and S. Coen, Appl. Phys. B **81**, 337-342 (2005).
18. N. Akhmediev and M. Karlsson, Phys. Rev. A **51**, 2602-2607 (1995).
19. F. Biancalana, D. V. Skryabin, and A. V. Yulin, Phys. Rev. E **70**, 016615 (2004).
20. P. V. Mamyshev, P. G. J. Wigley, J. Wilson, G. I. Stegeman, V. A. Semenov, E. M. Dianov, and S. I. Miroshnichenko, Phys. Rev. Lett. **71**, 73-76 (1993).